This is a repository copy of *Thermal performance of calcium-rich alkali-activated materials: A microstructural and mechanical study*.

White Rose Research Online URL for this paper:
http://eprints.whiterose.ac.uk/120425/

Version: Accepted Version

Article:

Kashani, A., Ngo, T.D., Walkley, B. orcid.org/0000-0003-1069-1362 et al. (1 more author) (2017) Thermal performance of calcium-rich alkali-activated materials: A microstructural and mechanical study. Construction and Building Materials, 153. pp. 225-237. ISSN 0950-0618

https://doi.org/10.1016/j.conbuildmat.2017.07.119

Article available under the terms of the CC-BY-NC-ND licence (https://creativecommons.org/licenses/by-nc-nd/4.0/).

Reuse
This article is distributed under the terms of the Creative Commons Attribution-NonCommercial-NoDerivs (CC BY-NC-ND) licence. This licence only allows you to download this work and share it with others as long as you credit the authors, but you can’t change the article in any way or use it commercially. More information and the full terms of the licence here: https://creativecommons.org/licenses/

Takedown
If you consider content in White Rose Research Online to be in breach of UK law, please notify us by emailing eprints@whiterose.ac.uk including the URL of the record and the reason for the withdrawal request.

eprints@whiterose.ac.uk
https://eprints.whiterose.ac.uk/

*Manuscript
Click here to view linked References

Thermal performance of calcium-rich alkali-activated materials: A microstructural and mechanical study

Alireza Kashani[1], Tuan D Ngo[1*], Brant Walkley[2], Priyan Mendis[1]

[1] Department of Infrastructure Engineering, The University of Melbourne, Victoria 3010, Australia

[2] Department of Materials Science and Engineering, The University of Sheffield, Sheffield S1 3JD, United Kingdom

* Corresponding author's email: dtngo@unimelb.edu.au

Abstract

The effects of Si/Al, Na/Al and water/solids ratios on thermal performance of alkali-activated materials (AAM) based on fly ash-slag blends are investigated. Higher Na/Al decreased compressive strength but increased post-heated strength retention and mass loss while reducing cracking at 1000°C. Lower Si/Al resulted in lowest initial strength but highest thermal stability, with an increase in strength after exposure to 1000°C, while a high degree of cracking was observed at higher Si/Al ratio. The effect of w/s on thermal performance was subtle. Computed tomography analysis showed for the first time thermally induced expansion of pores which reduced surface cracking via water vapour pressure release. Thermal performance of alkali-activated materials (AAM) is significantly better than Portland cement (PC) of the same compressive strength because of the very low bound water content. The porosity, pore connectivity and number of pores of the AAM were considerably higher than those in the PC binder.

Keywords: Microstructure; Tomography Analysis; Thermal Analysis; Mechanical Properties; Alkali-activated Materials; Geopolymer; Portland Cement

1. Introduction

Alkali activation of aluminosilicate-based materials such as blast furnace slag, fly ash, or metakaolin (collectively referred to as alkali-activated materials, AAM) can produce a binder with ~80-90% less associated CO_2 emissions and mechanical and durability properties comparable with or exceeding those of Portland cement (PC) [1]. Calcium-free and low-calcium alkali-activated aluminosilicate materials, also known as geopolymers, exhibit excellent resistance to fire and thermal stresses, evidenced by higher strength retention, a reduction in severity of cracking and an absence of spalling at an elevated temperature when compared to traditional PC binders [2]. Some AAM systems, however, exhibit poor thermal performance and fire-resistance [3, 4]. The thermal behaviour of AAM depends primarily on the chemistry and microstructure of the binder and consequently cannot be generalised across different binder systems [5]. Low-calcium AAM showed enhanced thermal stability due to lower bound water content within the gel when compared with PC [6]; bound water forms an essential part of the calcium silicate hydrate (C-S-H) gel and portlandite (CaOH) microstructure in hydrated PC [7] whereas the sodium aluminosilicate hydrate (N-A-S-(H)) gel formed in low-calcium AAM activated with sodium silicate or sodium hydroxide contains unbound water inside the pore network (i.e. pore solution) and hydroxyl groups adsorbed to the gel surface [8-10]. Low-calcium AAM systems, however, generally show lower ambient-cured mechanical strength than high-calcium AAM systems [11]. Inclusion of ground granulated blast furnace slag (GGBFS), which enriches the calcium content of the system and promotes formation of an alkali- and aluminium-substituted calcium silicate hydrate (C-(N)-A-S-H) gel or C-(N)-A-S-H/N-A-S-(H) gel blends upon alkali activation[12], has been shown to improve the performance of metakaolin-based AAM below 800°C [13].

Strong performance at higher temperatures is also attributed to the ability of the binder to form a network of interconnected pores which allow permeation of trapped steam to the

surface of the binder. Transport of steam to the surface markedly reduces cracking and spalling by reducing the pressure build-up of water vapour in closed pores [14, 15]. Lower thermal conductivity and sintering at elevated temperature has also been reported as reasons for increased fire-resistance properties of AAM compared to PC binders, which show rapid loss of strength at temperatures above 450°C [2]. With proper AAM formulation and curing, outstanding thermal stability is achieved by retaining the amorphous gel structure at high temperatures [2]. Poorly cured AAM with remnant unreacted alkali and silicates or excess water content, however, exhibit poor thermal stability at elevated temperatures, with gel devitrification above 800°C driving formation of a variety of crystalline phases [6, 16]. Bakharev [4] found that the strength of fly ash-based AAM systems deteriorated at temperatures above 800°C, in stark contrast to the observed increase in strength with increasing temperature (up to 800°C). Higher curing pressure was also observed to increase strength at ambient temperature as well as post-heat shrinkage while reducing strength retention at elevated temperatures as a result of reduced porosity [4].

At elevated temperatures, thermally-induced shrinkage of alkali-activated fly ash binders coincides with the thermal expansion of aggregate and results in substantial damage and strength loss (with strength loss proportional to aggregate size) [17, 18]. This shrinkage can be reduced, however, by the inclusion of alumina-based inorganic fillers in the binder [19]. Thermal shrinkage of alkali-activated metakaolin binders has been shown to increase with Si/Al ratio, and at lower Si/Al ratio is higher when the alkali cation is sodium compared to potassium [20]. At higher Si/Al, however, differences in charge-balancing alkali cations within the binder induce subtle changes in thermal shrinkage behaviour [20]. Thermal shrinkage of AAM has also been shown to increase with increasing water/solids (w/s) ratio and sodium content [4]. Potassium aluminosilicate hydrate- (K-A-S-(H)) based AAM systems exhibit increased post-heat strength up to 1000°C but lower ambient temperature

strength when compared to N-A-S-(H)-based systems due to the formation of crystalline phases, increased porosity and cracking at higher temperatures in N-A-S-(H) AAM [4]. The performance of alkali-activated fly ash [21] and fibre-reinforced alkali-activated metakaolin [22] samples (exhibiting a range of microstructures from porous to solid) were studied under simulated fire conditions. Despite the lower thermal conductivity of porous samples, the fire rating of solid AAM samples was higher. Phases that do not participate in alkali aluminosilicate gel formation have also been shown to affect performance at higher temperatures. Iron-rich phases which have higher thermal expansion compared to the N-A-S-(H) gel have been shown to cause cracking at elevated temperature, however crystalline silica phases were found to have a negligible effect on the thermal performance of alkali-activated fly ash [23].

In addition to thermally-induced chemical and atomic- or nano-structural changes in the gel, thermally-induced microstructural changes dictating porosity and permeability also play a significant role in thermal performance. Neutron pair distribution function (PDF) analysis showed that the alkali aluminosilicate gel ((N,K)-A-S-(H)) structure exhibited only subtle changes after heat exposure up to 1000ºC, and the majority of evaporated water in alkali-activated metakaolin binders results from water present in large pores and associated with hydration of alkali cations [23]. Sintering and densification of the AAM binder at elevated temperatures reduce pore accessibility and limits the ability of traditional gas-adsorption porosimetry (i.e. Brunauer–Emmett–Teller theory) to characterise the pore structure after exposure to elevated temperatures [24]. Micro-computed tomography (µ-CT), however, is able to resolve the majority of the pore structure above 30 µm in equivalent diameter in both AAM and PC binders exposed to elevated temperature [5].

Despite an abundance of studies examining the thermal performance of low-calcium AAM (using either metakaolin or low-calcium fly ash precursors), there has been limited previous

work examining thermal performance in high-calcium AAM systems based on GGBFS [25-27], and no previous work examining the thermal performance of alkali-activated fly ash-slag blends. Here, we examine the thermal performance of high-calcium AAM systems with fixed CaO content, varying Si/Al, Na/Al and w/s in the reaction mixture. These compositional parameters have been shown to be the main factors dictating the microstructure and mechanical performance of AAM [1], and are varied to investigate the resultant compositional and microstructural (including crystallinity, porosity and permeability) changes and their effects on compressive strength, elastic modulus and other physical properties in these systems at elevated temperature. In particular, a detailed discussion of the influence of porosity, pore connectivity, crack development and pore size on thermal performance within these systems is provided by application of micro computed tomography (μ-CT), thermogravimetric analysis and physical property characterisation. A comparison of the thermal performance of an AAM and a Portland cement binder with the same ambient-cured strength and water to solids ratio was also performed. This study provides for the first time a comprehensive investigation of the effect of precursor chemistry, gel composition and microstructure on thermal performance to provide a novel and enhanced understanding of the fundamental interactions which dictate the structure, strength and performance of AAM systems during exposure to elevated temperatures.

2. Materials and methods

GGBFS (hereinafter slag) and a commercially available blend of high-calcium fly ash (based on fly ashes from Gladstone and Callide power stations, Australia) were purchased from Cement Australia (chemical composition displayed in Table 1); X-ray fluorescence (XRF) analysis showed a loss on ignition at 1000°C of both precursors was negligible. A general purpose PC was purchased from Boral Australia.

Table 1. Chemical composition (weight percentage) of the fly ash and slag used, as determined by XRF

	Na_2O	MgO	Al_2O_3	SiO_2	P_2O_5	SO_3	K_2O	CaO	TiO_2	MnO	Fe_2O_3	Total
Fly Ash	0.81	1.27	25.13	42.09	1.10	0.41	0.41	13.56	1.44	0.18	13.16	100
Slag	1.51	5.56	14.01	32.83	0.07	2.28	0.35	41.9	0.53	0.22	0.50	100

Activating solutions were produced by dissolving solid sodium hydroxide (analytical grade with 99.9% purity, Chem-Supply, Australia) in water and subsequent addition of sodium silicate solution (Grade D, 9.4 wt.% SiO_2, 14.7 wt.% Na_2O and 55.9 wt.% H_2O, molar ratio SiO_2/Na_2O = 2, density = 1530 kg/m^3, viscosity = 400 cps, PQ Australia). Eight AAM samples of differing composition were produced by dry mixing fly ash and slag in a 4:1 ratio before addition of pre-prepared activating solutions (Table 2). Each sample code starts with G then the next number after it is the Si/Al molar ratio and the number in parenthesis is the Na/Al molar ratio. For instance, G2.1(0.65) has a nominal Si/Al ratio of 2.1 and nominal Na/Al of 0.65. A water to solids (w/s) ratio of 0.35 was used unless it was noted after the sample code (e.g. 37 for w/s of 0.37). A PC sample with w/s of 0.35 was cast for comparison. After 10 minutes mixing using a Hobart mixer, samples were cast into moulds. A vibrating table was used for 5 minutes in order to compact the paste and release any entrained air. Samples were sealed in plastic bags and cured at ambient temperature (25±2 °C) until the time of testing i.e. 14 days. 50 mm and 10 mm cubic samples were cast for compression tests and µ-CT scans, respectively.

Table 2. Reaction mixture composition for each sample

	G2.1(0.65)	G2.1(0.65)-33	G2.1(0.65)-37	G2.1(0.85)	G2.1(1)	G2.1(1.15)	G1.85(1)	G2.35(1)
Si/Al	2.10	2.10	2.10	2.10	2.10	2.10	1.85	2.35
Na/Al	0.65	0.65	0.65	0.85	1.00	1.15	1.00	1.00
w/s	0.35	0.33	0.37	0.35	0.35	0.35	0.35	0.35

Crystalline phases in the slag and fly ash precursors were neglected when calculating the mix proportions. Quartz, mullite and various iron rich crystalline phases (e.g. hematite) have been shown to be insoluble during alkali-activation over the time scale examined in this study, and consequently, only the amorphous component is considered reactive [28]. Quantitative X-ray diffraction (Q-XRD) analysis was used to calculate the amorphous portion of each phase (Table 3). The amorphous portion of the precursors as determined by Q-XRD does not necessarily indicate the total amount of reactive material (e.g. Ca present in crystalline phases such as gypsum can be reactive, and entrapment of amorphous material within insoluble crystalline phases can prevent reaction of it [29]), rather it provides an indication of the reactive precursor content. Diffraction data were collected using a Bruker D8 Advance instrument with Ni-filtered Co kα radiation (1.79 Å). Data were collected between 5 - 85° 2θ, with a step size of 0.02°, the scan rate of 1.0 s/step and spinning at 15 rpm. An anti-scatter blade was used to reduce the diffracted background intensity at low angles and an incident beam divergence of 1.0mm and 2.5° soller slit in the diffracted beam were used. Phase identification was completed using Diffrac. EVA V4.1 software with the ICDD PDF4+ 2015 database and Phase Quantification and Relative crystallinity was carried out using Bruker Diffracplus Topas software between 13° and 85° 2θ. The background was calculated using Chebychev method [30] with a single coefficient. Crystalline peaks were those identified as crystalline phases. The amorphous phase was determined using a single peak initially set with a Lorentzian crystallite size of 1ηm, with position and intensity refined to calculate the amorphous area.

Table 3. Chemical composition of crystalline phases in fly ash and slag (weight percentage with uncertainty of ± 2%), as determined by Q-XRD

Phase	Chemical Composition	Fly Ash	Slag
Calcite	$CaCO_3$	2.7	-
Hatruite	$Ca_3(SiO_4)O$	3.5	5.0
Brushite	$CaHPO_4 \cdot 2H_2O$	-	2.0
Gypsum	$CaSO_4 \cdot 2H_2O$	0.8	6.0
Hematite	Fe_2O_3	2.6	-
Magnesium Iron Oxide	$MgFe_2O_4$	2.4	-
Mullite	$Al_6Si_2O_{13}$	9.6	-
Quartz	SiO_2	2.9	-
Amorphous		75.5	87.0
Total		100	100

Compressive strength was measured using a universal testing instrument (ELE-international) with a displacement rate of 1 mm/min. Two parallel surfaces of the cubic samples were flattened using sand paper before applying the load. The maximum force that resulted in the failure of the sample was divided by the surface area to calculate compressive strength. Six 50mm cubes from each formulation were tested at 14 days of age and the results averaged. A supplementary compressive test using an Instron 5569A machine for assessment of the elastic modulus was used on 10 mm cubes (the smaller sample was used due to the maximum force limits of the instrument). The elastic modulus was calculated from the slope of the linear relationship (R^2>99.8%) between compressive stress and strain in the plastic region before sample failure. Three cubes from each sample were tested and the results averaged. Pieces of the crushed samples after the compression tests were ground using a pestle and mortar immediately after the test to form a fine powder (approximately 10 g) which was washed with acetone and filtered to remove free and loosely bound water and halt the

reaction (this method does not induce any significant changes in gel microstructure [31]). The dried powder was stored in sealed plastic tubes and stored in a desiccator to be used for thermogravimetric analysis (TGA). TGA was performed on powdered samples in an alumina crucible using a Perkin Elmer Diamond instrument and a heating rate of 6.60ºC/min. Samples were heated from 20°C to 110°C and held at this temperature for 60 minutes to allow equilibration, before being heated to 1000°C, held at this temperature for 60 minutes to allow equilibration and then cooled to ambient temperature.

An electric furnace was used to heat the samples to 1000°C to evaluate the appearance and mechanical properties of the samples after exposure to elevated temperatures. Six 50 mm cubic samples cured for 14 days were placed in the furnace so that only the bottom surface was contacted and heat exposure to the other surfaces was through air convection. The samples were heated using a similar regime to TGA experiments; heating at 6.6°C/min to 1000°C, holding at this temperature for one hour before cooling at 6.6°C/min to ambient temperature. Compressive strength tests were performed on heated samples immediately after cooling to room temperature using the same instrument and parameters as for ambient-cured samples.

Micro-computed tomography (µCT) data were obtained using a Phoenix Nanotom m (GE Sensing & Inspection Technologies GmbH, Wunstorf, Germany) operated using xs control and Phoenix datos|x acquisition software. Cubic samples of 1 cm^3 volume were mounted on glass rods and positioned on the micro-CT stage as close to the X-ray source as possible to achieve 2.67 micrometer resolution on a small subsection (6.36 × 6.36 × 6.36 mm) at the centre of the cubes. Samples were scanned for 60 minutes (timing = 750 mS, av = 2, skip =0) at 70kV and 160µA, collecting 2000 x-ray projections of each sample through 360° of rotation. Volume reconstruction of the micro-CT data was performed using Phoenix datos|x reconstruction software (GE Sensing & Inspection Technologies) and data was exported as

32-bit float volume files. This allowed for direct comparison of greyscale values in the histograms between data sets. A region of 1750×1750×1750 voxels in the centre of the sample was reconstructed, which was further cropped down to 1500×1500×1500 voxels after roughly registering the reconstructed data in order to match the same spot before and after exposure of the cubes to elevated temperature. Thus, the final dimensions used for analysis were 4×4×4 mm. Volume data was processed using Avizo (FEI). Porosity was segmented using the same region of the 32-bit grayscale histogram (-1 to 0.1) to produce binary images of the porosity in the sample. The volume fraction of segmented pore space was then computed by x-y slice through every x-y plane (1500 slices). Spherical pore size analysis and 3D restructuring of pores were conducted in order to measure pore size distribution and to calculate number of pores. Porosity and pore size have been shown to reduce as alkali-activated fly ash systems age [32] and consequently, samples of the same age were used for µ-CT scanning to avoid any age-induced variations.

3. Results and discussion

3.1. Effect of Na/Al ratio on AAM thermal performance

After exposure of all AAM samples to 1000°C, cracking and a colour change (from dark grey to light brown) was observed on the surface of each binder (Figure 1). When AAM samples were exposed to high temperature in a nitrogen atmosphere, no colour change was observed (Figure 2). The change of colour is consequently attributed to oxidation of iron species contained within fly ash particles during heating [3]. The content of iron species in the AAM mixture used in this study was approximately 10.4 wt. % (13 wt. % of fly ash precursor).

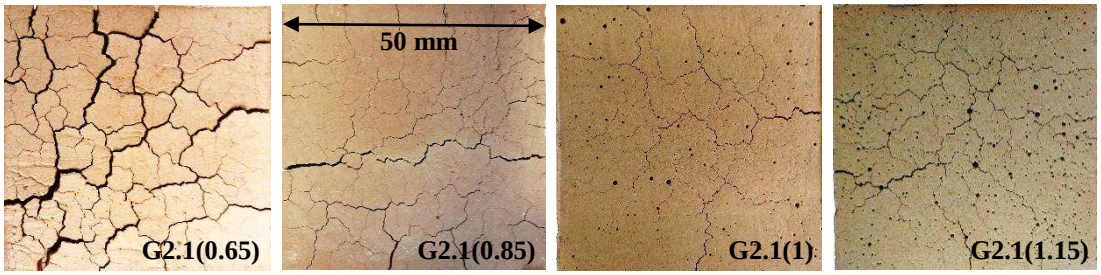

Figure 1. Surface of AAM cubes exposed to 1000°C (constant Si/Al of 2.1 and Na/Al is increased from 0.65 to 1.15)

Figure 2. Photos of G2.35(1) (highest Si/Al ratio of all AAM samples) after exposure to 1000°C; under nitrogen exposure (left) and under air exposure (right)

The intensity and depth of cracks were severe for the lowest Na/Al ratio of 0.65 but it was reduced at higher Na/Al ratios (Figure 1). Thermally-induced cracking occurs via a number of mechanisms. Water vapour in the AAM pore network has less chance of escape if surrounded by a dense matrix that has low permeability, and the consequent high pressure at higher temperatures results in cracking at the surface of the material [33]. Incongruent thermal shrinkage (e.g. of the gel) or expansion (e.g. of heterogeneous phases) caused by devitrification, sintering and other microstructural changes at higher temperatures also result in crack development and propagation [21]. It is likely that all three of these mechanisms are occurring here.

Fe_2O_3-containing phases do not participate in the alkali-activation reaction and are present in the binders in remnant unreacted fly ash particles [34]. These species have higher thermal coefficients of expansion compared to AAM paste and oxidation of these species at elevated

temperatures results in an increase in volume, formation of cracks at the interface between iron-rich spots and AAM gel, and a consequent reduction in mechanical strength [29]. Swelling and cracking after exposure to elevated temperatures has also been observed for fly ashes containing significant quantities of crystalline quartz phases [29, 35]. The amount of quartz in the system studied here, however, is very low and it is consequently unlikely that the cracks observed are due to the expansion of quartz. As such, the observed colour change (discussed above) and cracking attributed to oxidation of iron within the sample and/or incongruent shrinkage-expansion of different phases of the binder at high temperature [29, 36, 37].

The compressive strength of all samples decreased after exposure to 1000°C (Figure 3). Despite higher ambient-temperature compressive strength for samples with lower Na/Al ratio, the strength of these samples after heat treatment decreased significantly, with the magnitude the strength loss inversely proportional to the Na/Al ratio (and correlating with the extent of cracking discussed). Post-heated strength decreased (relative to ambient temperature strength) in samples with Na/Al > 1 (~10% strength reduction) and was very low compared with samples with Na/Al = 0.65 (~60% strength reduction). The compressive strength of ambient temperature samples also decreased with increasing Na/Al ratio from 0.65 to 1.15 (Figure 3). Lower alkalinity has been shown to drive formation of the C-(N)-(A)-S-H type gel in addition to the N-A-S-(H) gel and increase the mechanical performance of blended metakaolin/slag-based AAMs [38] and is likely to be contributing here.

In a low-calcium AAM systems (e.g alkali-activated low-calcium fly ash or metakaolin), a Na/Al molar ratio of 1 is required to completely counter-balance the negative charge of tetrahedral Al^{3+} atoms in the N-A-S-(H) gel. However, in calcium-rich AAM systems, high calcium content drives the formation of C-(N)-A-S-H at the expense of N-A-S-(H), increasing the compressive strength of the system. Ca-rich AAM exhibit lower thermal

stability compared to low-calcium AAM, which has a highly polymerised, three-dimensional gel framework and low content of bound water, as well as an absence of the water-rich phase Portlandite (CaOH) [6]. As a consequence of the increased water content in Ca-rich AAM, a significant drop in strength is observed after exposure to elevated temperature, contrasting with the higher ambient temperature compressive strength associated with these materials [38]. The thermal performance of the AAM samples investigated here is also dependent on porosity and pore size distribution (in turn affected by the Na/Al ratio of the binder); this will be discussed below in Section 3.4.

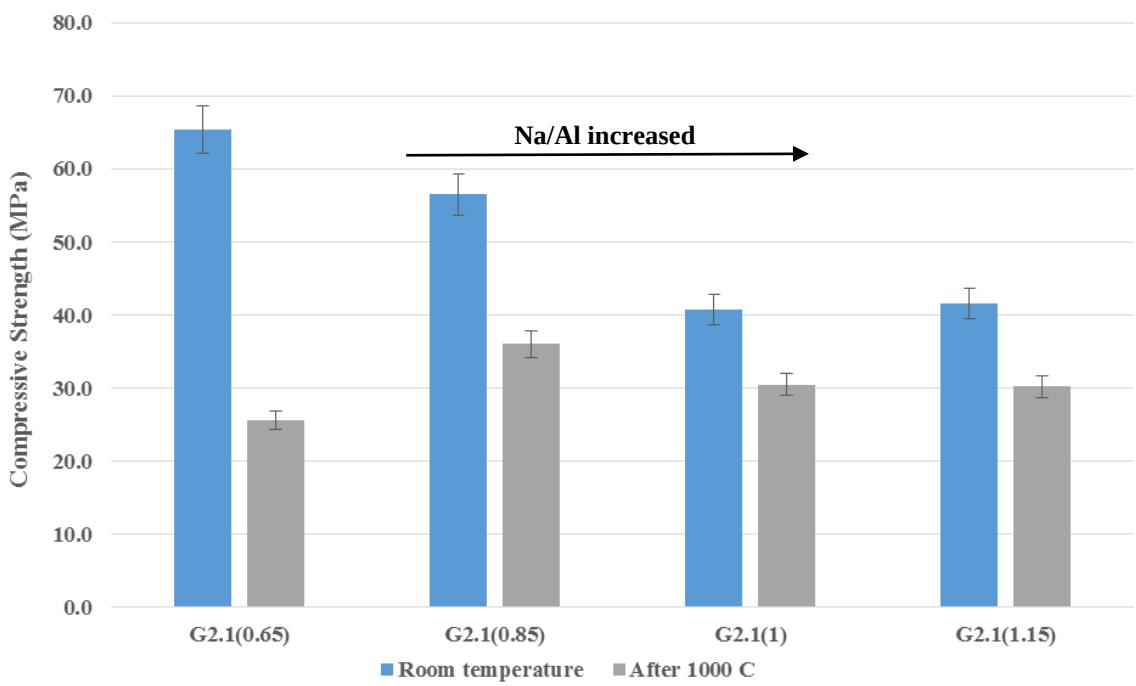

Figure 3. Compressive strength of AAM samples before and after exposure to 1000°C (constant Si/Al of 2.1 and Na/Al is increased from 0.65 to 1.15)

The total mass loss of each AAM sample during each heating segment as determined by TGA is shown in Figure 4. Between ambient temperature and 100 °C (Step 1 in Figure 4) mass loss occurs due to the removal of water adsorbed to the surface of the binder, moisture within the pore network and water loosely bound to the gel network [13, 39]. Higher amounts of

adsorbed, pore and loosely bound water are evident in samples with higher Na/Al ratio (end of Step 2 in Figure 4), consistent with the reduced bound water content of the N-A-S-(H) gel likely to have formed in these systems. As the same w/s ratio was used for all samples it can be concluded that amount of water that participated in the formation of hydrated products (e.g. N-A-S-(H) and C-(N)-A-S-H) was less compared to the sample with lower Na/Al In Step 3 (from 100 °C to 1000 °C) any remaining pore water will be removed, and as the temperature is increased dehydration and dehydroxylation of the reaction products (most likely N-A-S-(H) and C-(N)-A-S-H gels) will cause further mass loss [33, 40]. Bound water in the form of terminal hydroxyl groups on the N-A-S-(H) gel typically accounts for less than 5 wt. % of the total water content in metakaolin-based AAM [40]. Mass loss gradually increases with increasing alkali content (Figure 4), with G210115 exhibiting the highest mass loss after exposure to 1000°C, attributed to increased water molecules associated with hydration of Na^+ ions in the gels formed here [40].

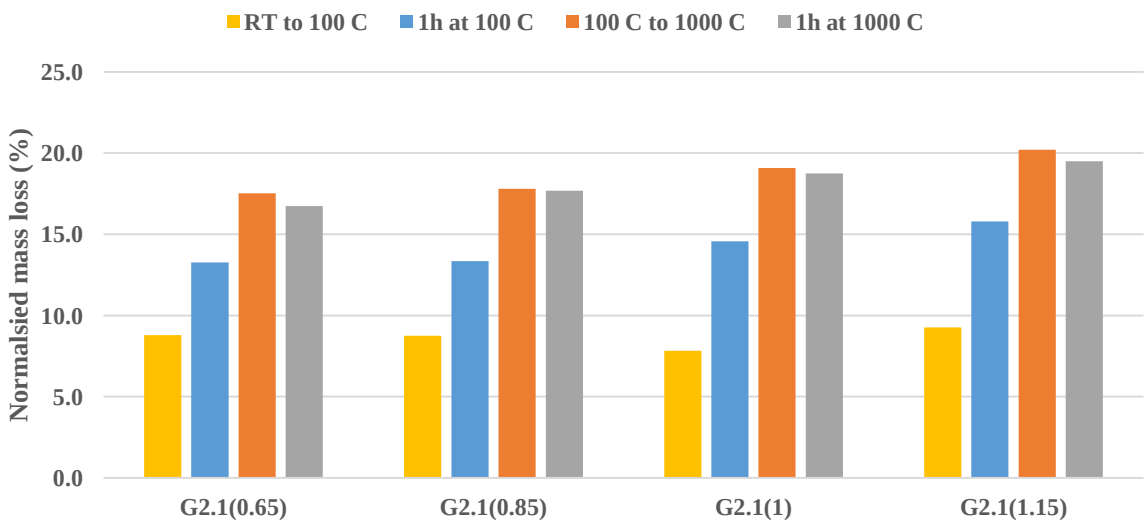

Figure 4. TGA mass loss of AAM samples (constant Si/Al of 2.1 and Na/Al is increased from 0.65 to 1.15)

3.2. Effect of Si/Al ratio on AAM thermal performance

The severity of cracks in AAM samples exposed to elevated temperature increased with Si/Al ratio (Figure 5). Residual silica provided by the activator which has not been incorporated into the reaction products (most likely N-A-S-(H) or C-(N)-A-S-H gels) may cause swelling and thermal instability at elevated temperatures [33, 36], and is the likely cause of the severe cracking observed in samples with high Si/Al ratio (Figure 5) [24]. As densification and viscous sintering occur during heating the AAM gel around the pores soften and collapse, resulting in cracking of the sample [41]. It follows that the highest degree of cracking was observed for the sample with the highest Si/Al ratio i.e. G235100, consistent with this mechanism.

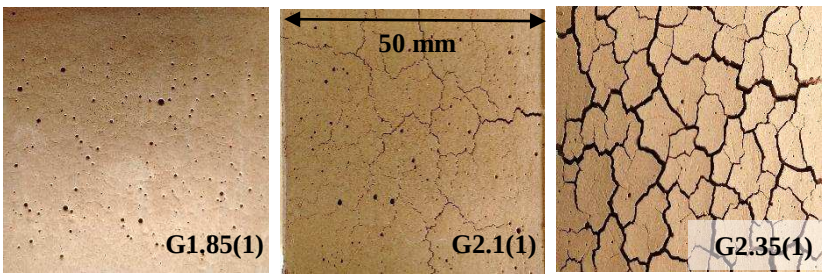

Figure 5. Surface of AAM cubes exposed to 1000°C (constant Na/Al ratio of 1 and Si/Al is increased from 1.85 to 2.35)

The compressive strength of ambient-cured AAM samples increases with increasing Si/Al ratio (Figure 6). This is consistent with a previous study in metakaolin-slag blends which showed increasing Si/Al ratio resulted in the formation of a calcium aluminium silicate hydrate (C-A-S-H gel) that coexists with the N-A-S-(H) (AAM) gel [38]. This increase in compressive strength in the samples investigated here is attributed to the formation of this C-A-S-H gel, in turn, driven by the presence of calcium-rich slag and higher availability of silica (higher Si/Al). It is also expected that a higher Si/Al ratio would increase the number of Si−O−Si bonds in the N-A-S-(H) gel (relative to Si−O−Al which are thermodynamically more susceptible to dissolution) [42]. Duxson, Provis, Lukey, Mallicoat, Kriven and van Deventer [42] showed the strength of a metakaolin-based AAM is maximised at Si/Al = 1.9

with Na/Al of unity. However, in the study, we present here the compressive strength increased with increasing Si/Al from Si/Al = 1.85 to 2.35, with Na/Al = 1. The metakaolin used in that study has the Si/Al ratio of 1.15 while here the Si/Al ratio of the mixture of precursors (fly ash and slag, 4:1) without activator is 1.7. The difference between Si/Al ratio of the highest strength mixture and metakaolin precursors in that study was 0.75 and in the current study is 0.65. Therefore, a possibility arises that the amount of silica added via the activator is more important than the Si/Al ratio of the final AAM mixture in the formation of high-strength AAM, particularly in nucleation of AAM reaction products [42]. This is consistent with previous observations that it is the dissolved Si which is freely available for the reaction that dictates gel structure, and therefore binder physical properties, in AAM [43, 44].In the presence of high Ca content, it is also possible that Si is being incorporated into C-(N)-A-S-H-type gel products which are likely to have formed here [38].

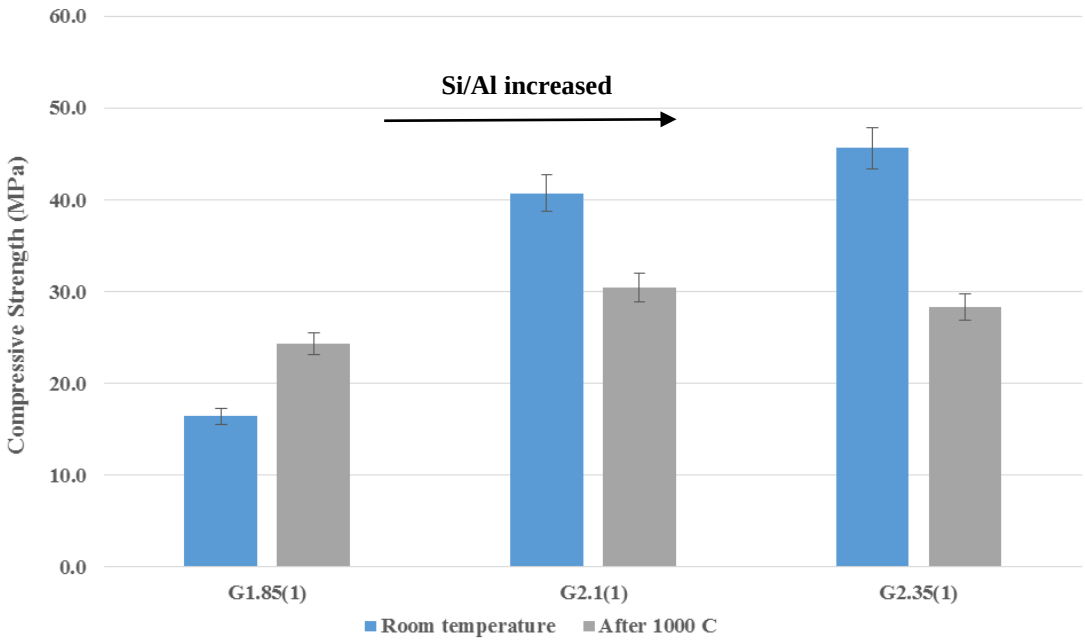

Figure 6. Compressive strength of AAM samples before and after exposure to 1000°C (constant Na/Al ratio of 1 and Si/Al is increased from 1.85 to 2.35)

Ambient temperature (before exposure to 1000°C) and post-heated (after exposure to 1000°C) compressive strength data for AAM samples of varying Si/Al ratio are shown in Figure 6. AAM sample G185100 (with the lowest Si/Al ratio) exhibited the best thermal stability, with substantial post-heated strength gain observed despite the very low ambient-cured strength for this sample. Previous work has shown that AAM samples that exhibiting significant increase in compressive strength after exposure to elevated temperatures have considerably lower ambient-cured strength, and vice versa [18, 19, 29, 36]. AAMs with less dense binder structures can resist volumetric changes during exposure to a high temperature without being damaged as the result of thermal shocks and dehydration, and this characteristic combined with gel devitrification at high temperature results in a significant increase in compressive strength [3]. Despite the higher ambient temperature strength exhibited by sample G235100 (which has the highest Si/Al ratio of all samples), post-heated strength retention in this sample was very low compared to samples with lower Si/Al, due to the high degree of thermal cracking which occurred in the dense binder structure.

Figure 7 shows a negligible difference in mass loss up to 1000°C (as determined by TGA) for AAM samples with varying Si/Al ratios, consistent with observations by Duxson, Lukey and van Deventer [24]. Interestingly, there is a substantial mass increase for sample G235100 after being held at 1000°C for an hour. By the end of this isothermal period, this sample had gained more than half the original mass loss. This mass gain does not occur when the same sample heated to 1000°C under the same temperature profile but within a nitrogen atmosphere purge (Figure 7), suggesting sample oxidation may be occurring during heating in air, which would be consistent the change of colour (from grey to light brown) observed for all samples and discussed in Section 3.1. However, the amount of Fe_2O_3 present in each sample was identical and if the mass gain was the cause of iron oxidation in air, it would be expected to occur for all samples, rather than just sample G2.35(1). Therefore, oxidation of

iron is unlikely to be the cause of this mass gain. Regardless of the actual cause, this mass gain is deemed responsible for the extensive post-heated cracking of sample G235100, consistent with previous observations of swelling and binder cracking due to excess silica in AAM systems [33, 36].

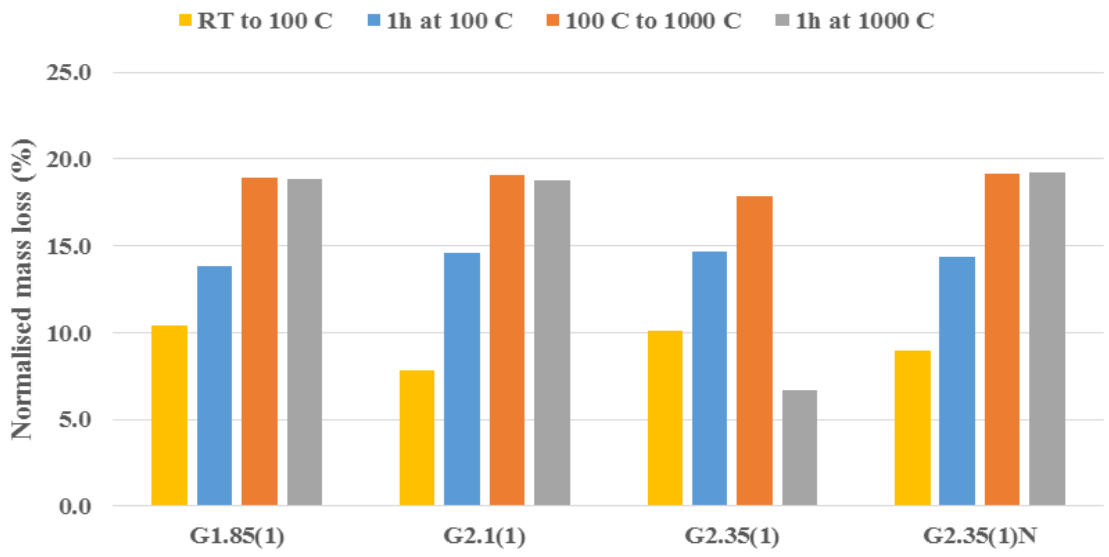

Figure 7. TGA mass loss of AAM samples (constant Na/Al ratio of 1 and Si/Al is increased from 1.85 to 2.35). N annotation indicates mass loss under nitrogen blanket)

3.3. Effect of water/solids ratio on AAM thermal performance

For AAM samples with different w/s ratios the difference in observed cracking was negligible (Figure 8), contrasting with previous work which showed increasing water content increased shrinkage and cracking in the AAM [4]. Increased w/s ratio for PC-based concrete, however, was shown to have negligible effects on post-heated mass loss and strength [45]. It can be concluded that regardless of the amount of water in the reaction mixture, the only water that is directly involved in gel formation (i.e. physically bound) or remains within the pore network will impact the elevated temperature performance. Very similar cross-sectional porosity distributions for w/s ratios of 0.33 and 0.37 (sample G210065-33 vs G210065-37) were observed using µ-CT analysis (Figure 9). It is possible that excess water in these

samples has come to the surface during sample vibration and drained, resulting in similar particle packing and pore networks which result in negligible differences in thermal performance. Consequently, the difference in water to solids ratio in the work presented here appears to allow improved workability (at higher w/s ratio) and ambient-cured strength (at lower w/s ratio) while having a negligible effect on thermal performance (Figure 10).

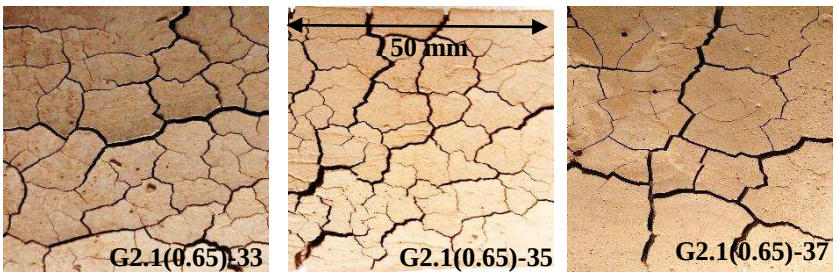

Figure 8. Surface of AAM cubes exposed to 1000°C (constant Si/Al of 2.1 and Na/Al of 0.65; w/s is increased from 0.33 to 0.37)

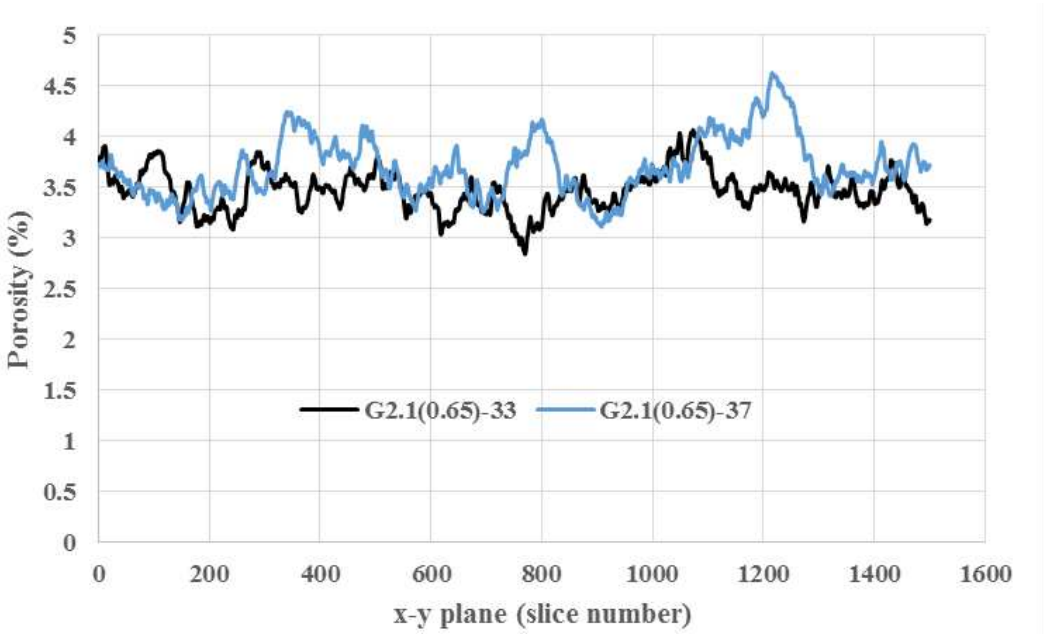

Figure 9. Porosity distribution of AAM samples with Si/Al of 2.1, Na/Al of 0.65 and different w/s ratios through 1500 slices of micro-CT data (x-y planes in 2.67 µm steps) along z-axis (height of the sample) at ambient temperature

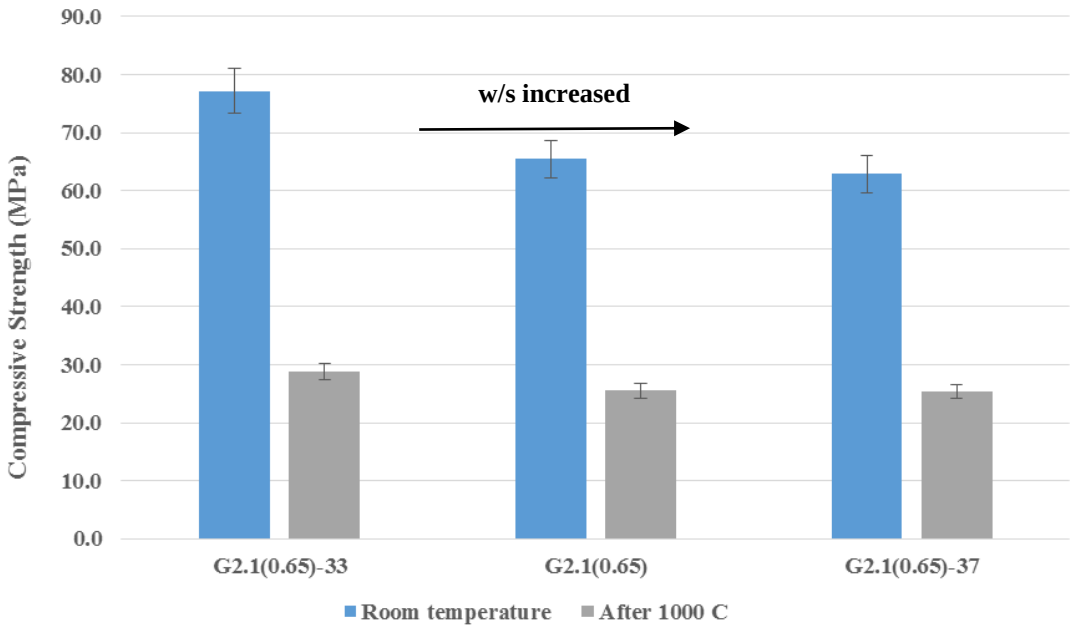

Figure 10. Compressive strength of AAM samples with Si/Al of 2.1 and Na/Al of 0.65 before and after exposure to 1000°C (w/s is increased from left to right)

3.4. Effect of porosity and pore size distribution on AAM thermal performance

At elevated temperature, high porosity has been shown to facilitate the release of water vapour from the AAM binder network, avoiding pressure build up and resisting against spalling [3, 15, 18]. Sample G185100 exhibited the highest initial porosity (Table 4), with no post-heated surface cracking or spalling observed in this sample. The high porosity and lower stiffness of this sample appear to allow the water vapour to escape the sample easily during heating by expanding the pores into thin pathways (~200 micrometres diameter) inside the sample (Figure 11). These pathways reduce the chance of spalling by releasing the water vapour before pressure build-up within the confined pores, which can damage the structure. No cracks were found on the surface of sample G185100 (Figure 5); instead, a number of holes can be observed on the surface; these are likely to be the ends of these pathways which allow the release of the water vapour. It has been shown that fly ash-based AAM samples with lower strength, less compact structure and higher permeability, similar to G185100 in

this study, are more resistant to dehydration damage compared to high-strength AAM samples with less permeability [3] consistent with observations here.

The temperature gradient between the surface and inner section of an AAM contributes substantially to cracking and damage at the binder surface [22]. These pathways observed here provide a mechanism to reduce this temperature gradient via convection of hot air, with severe cracking observed on the surface of other samples that did not exhibit these post-heated internal pathways.

Table 4. Porosity, mean and median diameter and number of pores of PC and AAM samples with varying Na/Al and Si/Al ratios from µ-CT data before and after exposure to 1000°C (ET: elevated temperature)

	Cement	Cement-ET	G2.1(0.65)	G2.1(0.65)-ET	G2.1(1)	G2.1(1)-ET	G1.85(1)	G1.85(1)-ET
Porosity (%)	**0.6**	**0.6**	**3.7**	**10.5**	**1.8**	**4.3**	**4.3**	**12.3**
Mean diameter (µm)	**4.7**	**11.0**	**5.6**	**6.3**	**5.7**	**6.9**	**5.6**	**7.5**
Median diameter (µm)	**3.3**	**4.8**	**4.1**	**4.7**	**4.2**	**4.2**	**4.2**	**4.7**
Total number of pores (x1000)	**134**	**17**	**5,373**	**5,623**	**1,588**	**1,083**	**2,113**	**879**
Volume fraction of pores under 50 µm (%)	**4**	**6**	**61**	**21**	**44**	**16**	**48**	**6**

The overall volume of the samples also plays a significant role in dictating cracking, with larger samples exhibiting more severe cracking due to restricted heat flow away from the sample and a resultant increased temperature gradient [18]. The 50 mm cubes used for compressive strength tests in this study developed larger post-heated cracks compared to the smaller 10 mm cubes used for µ-CT scan analysis. The same layer (x-y plane of µ-CT scan) inside the cube was monitored for selected samples before and after exposure to 1000°C (Figure 11). This shows the formation of micro-cracks is initiated from the surface of the sample, with less cracking observed in the sample interior. Because of the higher stiffness of

these samples, the micro-cracks cannot propagate through the sample interior and form pathways. Instead, the cracks get larger and propagate in the outer layer of the sample as shown in Figure 5. It must be noted that the region of interest for µ-CT images is a cube of length 4 mm inside the sample (which itself is a cube of length 10mm) that was exposed to elevated temperature. Therefore, the sides of the µ-CT images (Figure 11) do not align with the surfaces shown in Figure 5. The micro-cracks on the sides of µ-CT images are therefore only the internal ends of the larger surface cracks observed in Figure 5. Binders which were stiffer and less permeable are more prone to develop high internal tension at elevated temperatures due to the large water vapour pressure build-up. Permeability is related to the pore connectivity, and higher porosity does not always result in higher permeability. For instance, a sample with lower porosity with many isolated pores can result in more structural damage at elevated temperature compared to a sample with higher porosity but interconnected pores (higher permeability).

The porosity of the cement sample (w/s = 0.35) is considerably lower than that of all AAM systems investigated in this study (Table 4). This contrasts with observations by Rivera, Long, Weiss Jr, Moser, Williams, Torres-Cancel, Gore and Allison [5] who observed lower porosity for ambient-cured alkali-activated fly ash AAMs compared to PC using similar µ-CT analysis. It is possible that the difference in observed porosity is a result of differences in particle packing, which in turn is a result of variations in the particle size distributions of the precursors. It should also be noted that a system containing 100% fly ash has better particle packing than that of slag/fly-ash blends (due to the spherical nature of fly ash particles) [46]. Despite the differences in overall porosity, the number of pores in the AAM examined here were considerably higher than PC, consistent with observations by Rivera, Long, Weiss Jr, Moser, Williams, Torres-Cancel, Gore and Allison [5]. Therefore, the overall porosity and pore size distribution appear dependent on particle size distribution and packing and

consequently varies between not only PC and AAM but also between different AAM systems.

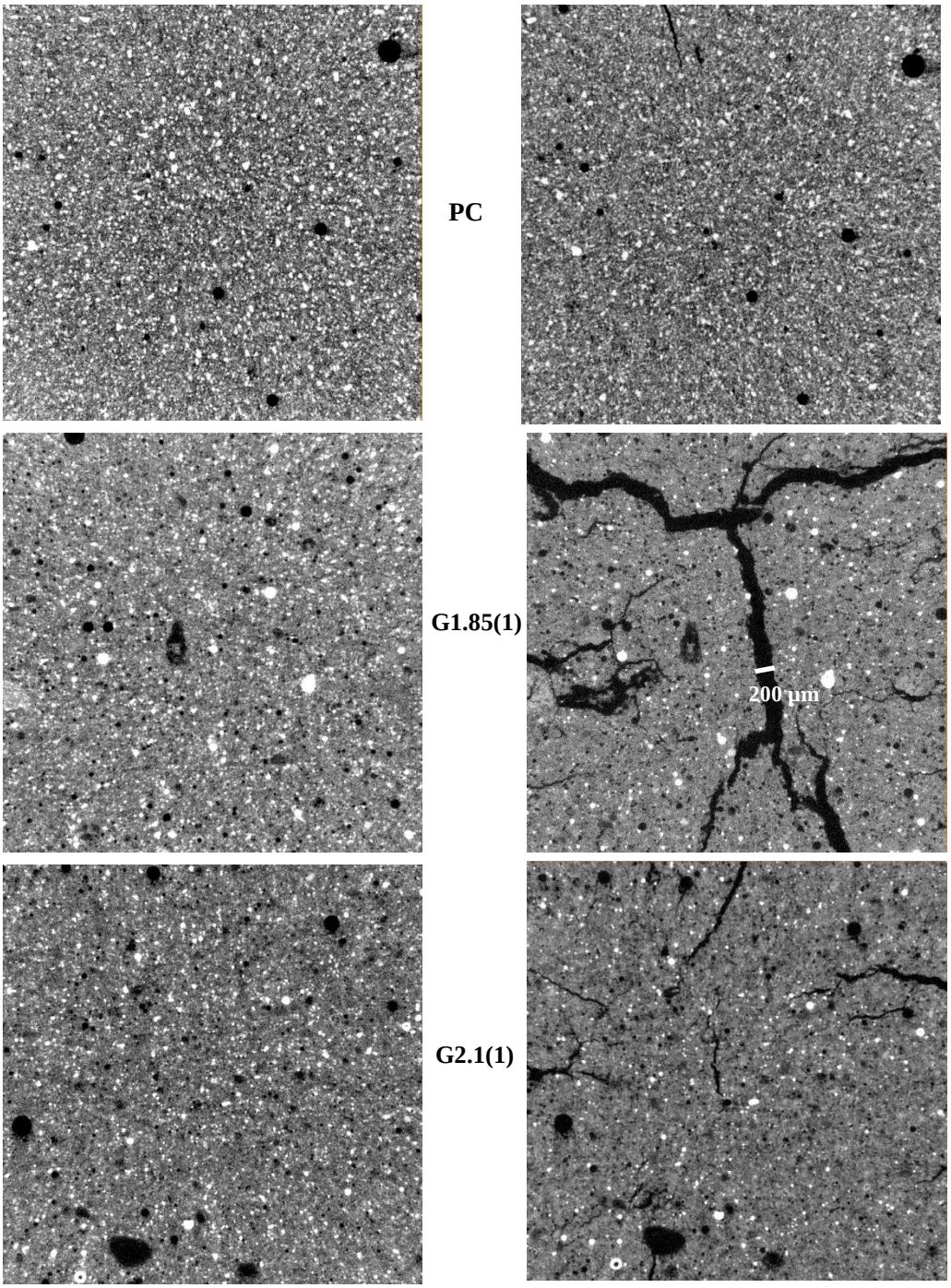

Figure 11. 2D µCT scan images of PC and AAM samples (with constant Na/Al of 1 and Si/Al of 1.85 and 2.1) before (left) and after (right) exposure to 1000°C (each photo represent 4 x 4 mm); pores are shown in black, dense phases in white and binder in grey

Changes in the mean and median diameters of pores in ambient temperature and post-heated AAM samples are shown in Table 4. In all systems, a large increase in pore size (pore coarsening) and total porosity is observed in samples exposed to 1000°C. The increase in pore diameter is more pronounced in PC compared to the AAM samples. This phenomenon is the primary cause of damage to PC binders exposed to elevated temperatures [47]. Pore coarsening at high temperature also results in a decrease in the total number of pores (where some pores expand and combine to form larger diameter pores). This is evident for the PC sample, where an increasing in the mean diameter of pores from 4.7µm to 11µm after heating resulted in a reduction in the number of pores in the scanned region by more than 90% (Table 4). The difference between ambient temperature and post-heated mean and median diameters of AAM samples was negligible, and this difference did not vary significantly with varying Si/Al or Na/Al ratio.

The number of pores, however, decreased substantially as Na/Al ratio was increased i.e. from 0.65 (sample G210065) to 1 (sample G210100). Despite these two samples having similar mean and median pore diameters, the higher number of pores in sample G210065 (lower Na/Al) results in a porosity approximately twice that of G210100 (higher Na/Al). An increase in the number of pores and porosity was also observed when decreasing Si/Al ratio from 2.1 to 1.85 (G210100 compared to G185100) as shown in Table 4. Higher alkali and higher silica content in alkali-activated fly ash systems have both been shown to result in a greater extent of reaction, resulting in finer pores and lower porosity [2, 32, 42]. The porosity of the sample with lower Si/Al ratio (G185100) is more than double of the sample with higher silica (G210100) at ambient temperature. An AAM system with a high content of unreacted precursor fly ash particles results in a porous structure due to a lower extent of reaction, therefore, lower amount of AAM gel which can fill pores between particles. This facilitates

the escape of water vapour at elevated temperatures and reduces cracking compared to AAMs with greater reaction product formation [36].

Figure 12 shows the distribution of pores with an equivalent diameter of greater than 50 micrometres within the region of interest (4mm cube) for selected samples at ambient temperature and after being exposed to 1000°C. The number of pores present in the PC sample is less than that for AAM samples. Also, pore connectivity in PC appears substantially lower than that in AAM systems, similar to previous observations [15]. The volume fraction of pores under 50 micrometre for PC is less than 5% (Table 4) and does not change after firing. This contrasts with the post-firing volume fraction for the selected AAM systems, which is almost half of pre-heated total pore volume. The size of smaller pores grows and some pores propagate and develop micro-cracks and larger diameter pores after exposure to 1000°C (Figure 12).

Figure 13 shows the porosity distribution along the length of each sample (derived from µ-CT) analysis of the PC and the selected AAM samples before and after exposure to 1000°C. For the PC sample, porosity remains low and similar pre- and post-heated porosity distributions were observed. The samples with the lowest Na/Al (G210065) and Si/Al (G185100) have the highest initial porosity, and this increased substantially after exposure to elevated temperature. However, after exposure to elevated temperature substantial loss of strength and cracks were observed for sample G210065, contrasting with the strength gain and absence of severe cracking observed for G185100 and demonstrating the effect of sample stiffness on thermal behaviour. Despite a similar porous structure, the higher strength in sample G210065 prevented an increase in pore diameter to release water vapour and avoid structure damages, as was observed with the very low-strength sample G185100. Indifference between pre- and post-heated porosity of sample G210100 (Si/Al of 2.1 and Na/Al of 1) were more subtle after compared to samples with lower Na/Al (G210065) and Si/Al (G185100).

G210100 also showed moderate strength loss and surface cracking compared to the other samples. Crack development after heat exposure for samples with higher strength is also indicated by sharp peaks in porosity distribution, as observed for G210065 in Figure 13.

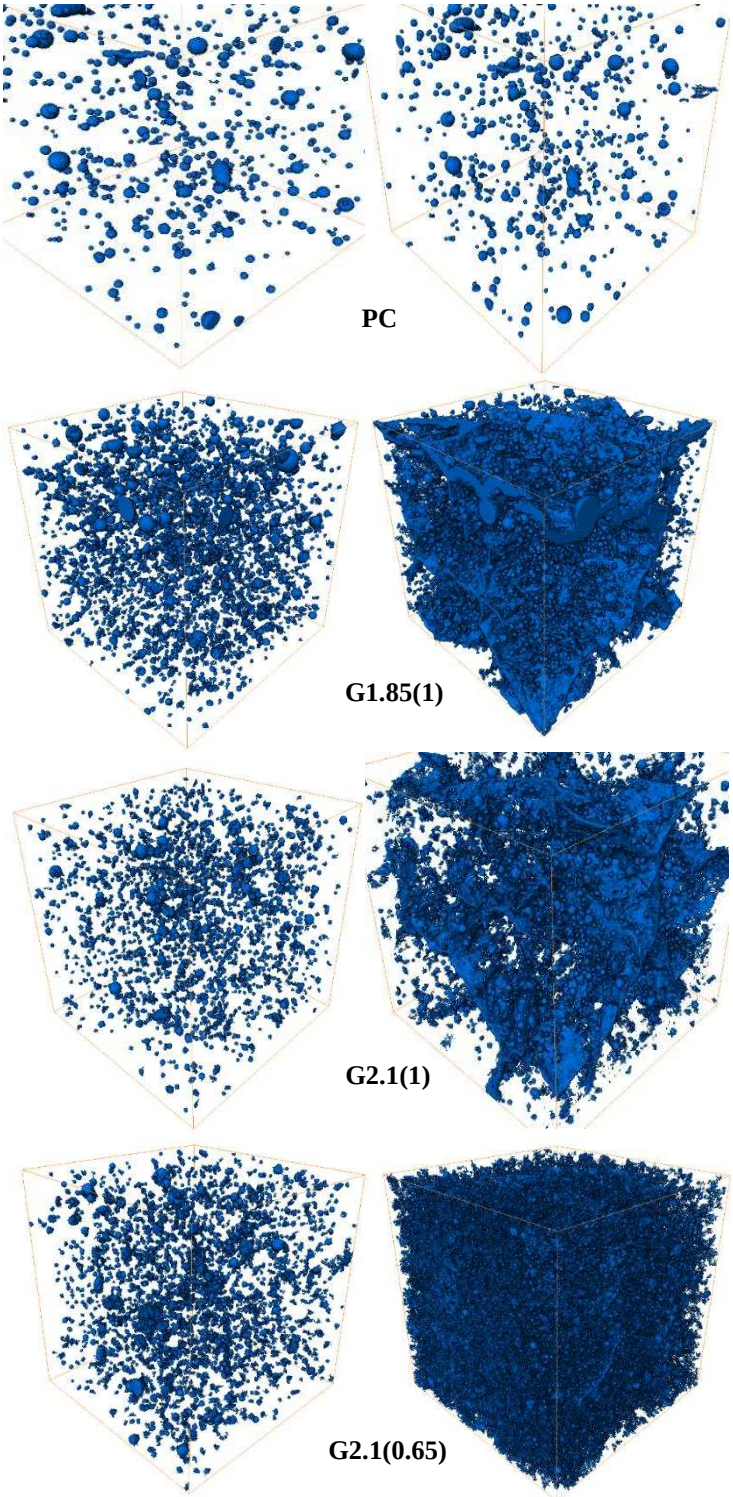

Figure 12. 3D µCT scan of pores in PC and AAM samples with different Na/Al and Si/Al ratios before (left) and after (right) exposure to 1000°C (each cube represent 4 x 4 x 4 mm);

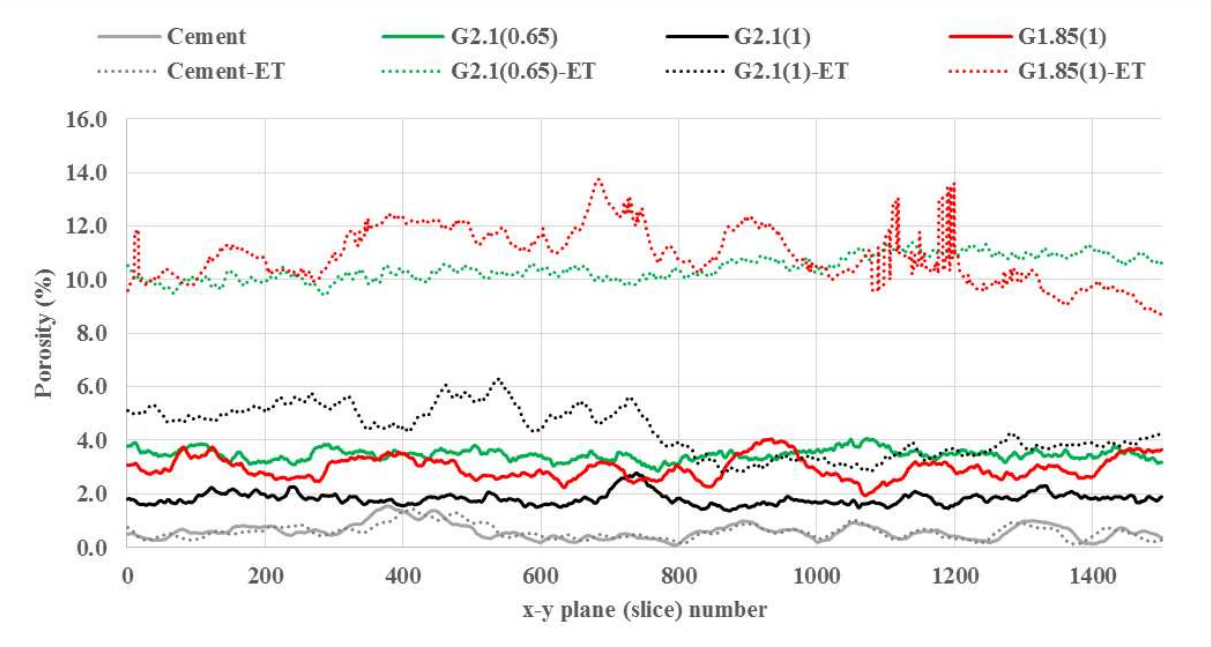

Figure 13. Porosity distribution of PC and AAM samples with different Na/Al and Si/Al ratios through 1500 slices of micro-CT data (x-y planes in 2.67 µm steps) along z-axis (height of the sample) before (solid line) and after (dotted line) exposure to 1000°C

3.5. Effect of composition on elastic modulus (stiffness) of AAM

No distinguishable trend was found between the elastic modulus of the samples with different compositions (Si/Al or Na/Al) (Table 5), consistent with previous findings that the elastic modulus of an AAM system is dictated by microstructural homogeneity rather than atomic composition and strength [42]. This contrasts with previous work on PC systems, which has shown that the elastic modulus decreases with increasing porosity of PC [47]. Samples with a higher elastic modulus showed lower strength retention and larger crack development at elevated temperature. The larger AAM binder volume allows stress to spread during compression and results in higher elastic modulus. The lower elastic modulus and compressive strength of G185100 compared to other samples is attributed to a lower rate of gel formation, in turn, due to lower dissolved silicate species provided by activator which is

required for nucleation and gel formation (due to the thermodynamic preference for Al dissolution from the precursor) [42].

Table 5. Elastic modulus of PC and AAM samples with different Na/Al and Si/Al ratios

Sample	Elastic modulus (MPa)
Effect of Na/Al	
G2.1(0.65)	3545
G2.1(0.85)	3985
G2.1(1)	2974
G2.1(1.15)	3120
Effect of Si/Al	
G1.85(1)	1928
G2.1(1)	2974
G2.3(1)	2935
PC	2942

3.6. A comparison between thermal performance cement and AAM mortars

For PC, water evaporation and dehydration of hydrated cement products (i.e. calcium silicate hydrate, Portlandite and ettringite), as well as higher binder stiffness, can cause cracking due to volumetric expansion induced stress within the binder [5, 45, 47, 48]. In contrast, White, Provis, Gordon, Riley, Proffen and van Deventer [40] showed firing above 800 ^{o}C has a minor impact on the AAM gel framework structure, with the elimination of terminal hydroxyl groups attached to the AAM gel framework being the only observable change. Higher temperature can result in densification and devitrification of the AAM gel which can improve the mechanical properties [2]. Thermal degradation of PC hydration products can cause structural damage and negatively affect post-heated mechanical properties [49]. Severe surface cracking was observed for sample G210065 (Figure 14 shows), which exhibited the same ambient temperature compressive strength as the PC sample. The compressive strength

of the PC sample decreased by approximately 90% after exposure to 1000 °C (Figure 15) compared to sample G210065 (Si/Al of 2.1 and Na/Al of 0.65) which had the considerably higher post-heated strength. This indicates that thermal degradation of PC hydration products causes significantly more damage to the mechanical properties compared to AAMs system with the same compressive strength, despite the limited thermally induced cracking and changes in porosity in PC samples.

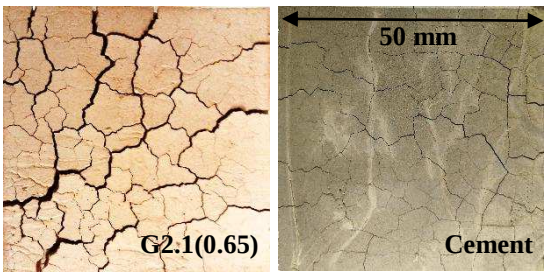

Figure 14. Surface of AAM (with Si/Al of 2.1 and Na/Al of 0.65) and cement cubes with the same w/s ratios exposed to 1000°C

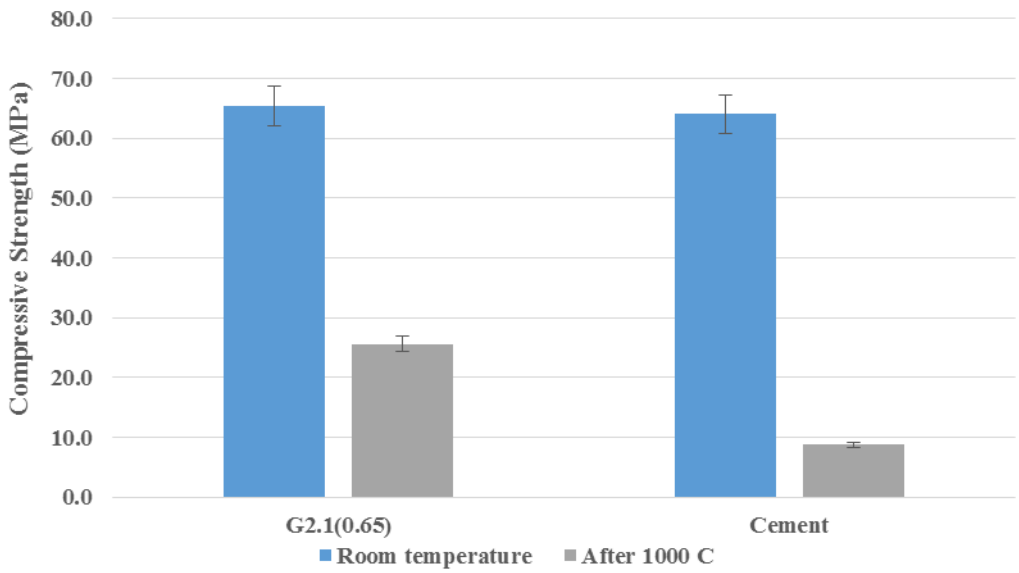

Figure 15. Compressive strength of AAM (with Si/Al of 2.1 and Na/Al of 0.65) and cement samples before and after exposure to 1000°C

Figure 16 shows a comparison of TGA data for the PC sample and AAM sample G210065. Both samples have the same nominal water content (w/s = 0.35). The mass loss associated with evaporation of water at low temperatures is very similar in both samples. The higher

mass loss above 100°C for the PC sample (compared to the AAM sample) is associated with the loss of free water and dehydration of ettringite, followed by dehydration of C-S-H between 200°C to 400°C and dehydration of Portlandite around 450°C [5, 47, 49]. For the AAM system, the mass loss above 100°C can be attributed to dehydration of C-(N)-A-S-H- and N-A-S-(H)-type products which are likely to have formed in the AAM as well as dehydroxylation of terminal hydroxyl groups in the AAM gel. No mass loss peak is observed in the region of 450°C confirming the expected absence of Portlandite, $Ca(OH)_2$, in the AAM gel. The mass loss associated with the presence of Portlandite was not found in TGA curves for all other AAM samples (data not shown). Therefore $Ca(OH)_2$ was not produced during alkali activation of the Ca-rich blended system despite very high alkalinity in some of the AAMs. No mass loss is observed beyond 700°C, consistent with previous studies of fly ash-based and fly ash/slag blended AAMs at elevated temperature [18, 38]. Higher mass loss after exposure to 1000°C reveals the existence of more chemically bonded water in the structure of hydrated PC compared to the Ca-rich AAM samples with the same strength and w/s ratio. This structural damage that results from thermal degradation of PC hydration products is the main reason for the inferior thermal performance of PC compared to the AAM binders [5].

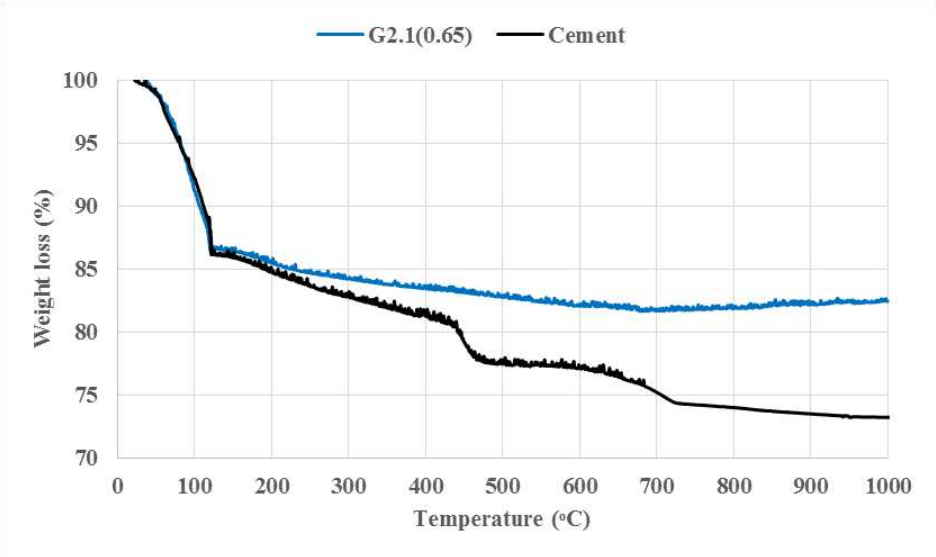

Figure 16. TGA mass loss of AAM (with Si/Al of 2.1 and Na/Al of 0.65) and cement samples as temperature increased up to 1000°C

3.7. The effect of density on AAM strength reduction at elevated temperature

A general trend was observed between density of concrete cubes and their post-heated strength reduction. G185100 exhibited the lowest ambient temperature and has the lowest density and post-heated strength gain. In contrast, the PC sample and AAM sample G210065 exhibited higher density and ambient temperature strength and showed a substantial decrease in post-heated strength. The dense structure and higher strength of these samples resulted in higher internal water vapour pressure which caused substantial damage to the structure. In addition, structural damage as a result of dehydration of PC hydration phases resulted in a 90% strength loss after firing, much higher than that observed in all AAM samples.

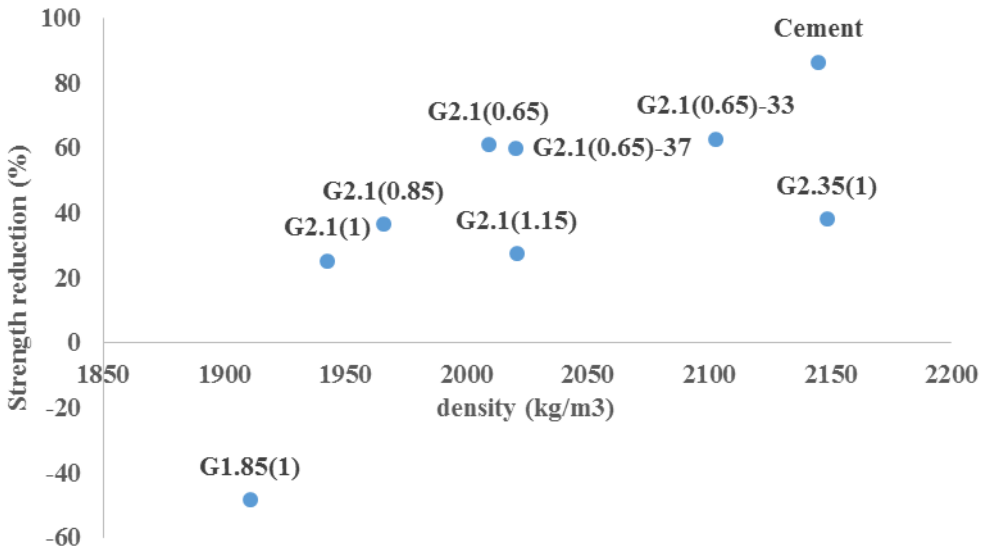

Figure 17. Strength reduction after exposure to 1000°C versus average density of AAM with different Na/Al and Si/Al ratios and PC samples (negative values mean strength gain)

4. Conclusions

The effects reaction mixture composition and water content on the mechanical, microstructural and thermal properties of a series of AAM were investigated. AAM was produced by alkali-activation of a blend of 80 wt. % fly ash and 20 wt% slag precursors

activated with different sodium silicate solutions and cured for 14 days at ambient temperature.

Post-heated surface cracking decreased with increased reaction mixture Na/Al ratio. Despite higher ambient temperature compressive strength for samples with lower Na/Al ratio, post-heated compressive strength was significantly reduced compared to samples with higher Na/Al ratio. Compressive strength increased with increasing Si/Al from 1.85 to 2.35 and Na/Al of unity. Lower AAM Si/Al ratio exhibited the best thermal stability, while a high degree of surface cracking was observed at higher Si/Al ratio. A negligible difference in mass loss up to 1000°C for AAM samples with different Si/Al ratios was observed, however a substantial mass gain due to possible oxidation reaction was observed for high Si/Al AAM during an isothermal period at 1000°C. W/s ratio did not affect post-heated surface cracking or porosity in AAM samples.

µ-CT analysis showed for the first time thermally induced expansion of pores into water-vapour pathways and pore coarsening, which substantially reduced post-heated surface cracking via water vapour pressure release and temperature gradient minimisation during heating. Less permeable and stiffer binders are more prone to develop higher internal tension because of the great extent of the built-up pressure of internal pore water at higher temperatures.

Variation in Si/Al or Na/Al ratio did not appear to affect mean and median pore diameters in the AAM. However, lower Na/Al and Si/Al increased both initial and post-heated porosity. The porosity, pore connectivity and number of pores (<50µm) of the AAM were considerably higher than those in the hydrated PC binder at the same w/s ratio. In all systems, an increase in porosity and pore size was observed after exposure to 1000°C.

Thermal performance of AAM binders is significantly better than that of PC binders of the same compressive strength. This is due to the very low content of bound water within the

AAM gel framework, which does not experience the same extent of structural damage as PC systems exposed to high temperatures, where structural damage occurs via dehydration of PC hydration products e.g Portlandite.

5. Acknowledgment

This project was funded through an Australian Research Council Linkage Project [Grant Number: LP140100504] and through the ARC Centre for Advanced Manufacturing of Prefabricated Housing. The authors acknowledge the support of the Trace Analysis for Chemical, Earth and Environmental Sciences (TrACEES) platform from the Melbourne Collaborative Infrastructure Research Program at the University of Melbourne and Dr Jay Black from School of Earth Sciences for assistance with μ-CT experiments. XRD analysis was performed in part at the Materials Characterisation and Fabrication Platform (MCFP), The University of Melbourne, and the Victorian Node of the Australian National Fabrication Facility (ANFF). The authors also acknowledge the use of laboratory facilities of the Geopolymer and Minerals Processing Group, The University of Melbourne.

6. References

[1] J.L. Provis, J.S.J. van Deventer, Alkali-activated materials: State-of-the-Art Report, Springer/RILEM, Berlin, 2013.

[2] L. Vickers, A.v. Riessen, W.D.A. Rickard, Fire-resistant geopolymers : role of fibres and fillers to enhance thermal properties, Springer, Singapore, 2015.

[3] W.D.A. Rickard, C.S. Kealley, A. van Riessen, Thermally Induced Microstructural Changes in Fly Ash Geopolymers: Experimental Results and Proposed Model, Journal of the American Ceramic Society 98(3) (2015) 929-939.

[4] T. Bakharev, Thermal behaviour of geopolymers prepared using class F fly ash and elevated temperature curing, Cement and Concrete Research 36(6) (2006) 1134-1147.

[5] O.G. Rivera, W.R. Long, C.A. Weiss Jr, R.D. Moser, B.A. Williams, K. Torres-Cancel, E.R. Gore, P.G. Allison, Effect of elevated temperature on alkali-activated geopolymeric binders compared to portland cement-based binders, Cement and Concrete Research 90 (2016) 43-51.

[6] V.F.F. Barbosa, K.J.D. MacKenzie, Synthesis and thermal behaviour of potassium sialate geopolymers, Materials Letters 57(9–10) (2003) 1477-1482.

[7] I.G. Richardson, The calcium silicate hydrates, Cement and Concrete Research 38(2) (2008) 137-158.

[8] J.L. Provis, S.A. Bernal, Geopolymers and related alkali-activated materials, Annual Review of Materials Research 44(1) (2014) 299-327.

[9] P. Duxson, A. Fernández-Jiménez, J.L. Provis, G.C. Lukey, A. Palomo, J.S.J. van Deventer, Geopolymer technology: the current state of the art, Journal of Materials Science 42(9) (2007) 2917-2933.

[10] A. Palomo, S. Alonso, A. Fernández-Jiménez, Alkaline activation of fly ashes: NMR study of the reaction products, Journal of the American Ceramic Society 87(6) (2004) 1141-1145.

[11] J. Temuujin, A. van Riessen, R. Williams, Influence of calcium compounds on the mechanical properties of fly ash geopolymer pastes, Journal of Hazardous Materials 167(1–3) (2009) 82-88.

[12] S.A. Bernal, J.L. Provis, B. Walkley, R. San Nicolas, J.D. Gehman, D.G. Brice, A.R. Kilcullen, P. Duxson, J.S.J. van Deventer, Gel nanostructure in alkali-activated binders based on slag and fly ash, and effects of accelerated carbonation, Cement and Concrete Research 53 (2013) 127-144.

[13] S.A. Bernal, E.D. Rodriguez, R.M. de Gutierrez, M. Gordillo, J.L. Provis, Mechanical and thermal characterisation of geopolymers based on silicate-activated metakaolin/slag blends, Journal of Materials Science 46(16) (2011) 5477-5486.

[14] R. Jansson, L. Boström, The Influence of Pressure in the Pore System on Fire Spalling of Concrete, Fire Technology 46(1) (2009) 217.

[15] R. Zhao, J.G. Sanjayan, Geopolymer and Portland cement concretes in simulated fire, Magazine of Concrete Research 63(3) (2011) 163-173.

[16] V.F.F. Barbosa, K.J.D. MacKenzie, Thermal behaviour of inorganic geopolymers and composites derived from sodium polysialate, Materials Research Bulletin 38(2) (2003) 319-331.

[17] D.L.Y. Kong, J.G. Sanjayan, Damage behavior of geopolymer composites exposed to elevated temperatures, Cement and Concrete Composites 30(10) (2008) 986-991.

[18] D.L.Y. Kong, J.G. Sanjayan, Effect of elevated temperatures on geopolymer paste, mortar and concrete, Cement and Concrete Research 40(2) (2010) 334-339.

[19] L. Vickers, W.D.A. Rickard, A. van Riessen, Strategies to control the high temperature shrinkage of fly ash based geopolymers, Thermochimica Acta 580 (2014) 20-27.

[20] P. Duxson, G.C. Lukey, J.S.J. van Deventer, Thermal evolution of metakaolin geopolymers: Part 1 – Physical evolution, Journal of Non-Crystalline Solids 352(52–54) (2006) 5541-5555.

[21] W.D.A. Rickard, A. van Riessen, Performance of solid and cellular structured fly ash geopolymers exposed to a simulated fire, Cement and Concrete Composites 48 (2014) 75-82.

[22] W.D.A. Rickard, L. Vickers, A. van Riessen, Performance of fibre reinforced, low density metakaolin geopolymers under simulated fire conditions, Applied Clay Science 73 (2013) 71-77.

[23] C.E. White, J.L. Provis, T. Proffen, J.S.J. Van Deventer, The Effects of Temperature on the Local Structure of Metakaolin-Based Geopolymer Binder: A Neutron Pair Distribution Function Investigation, Journal of the American Ceramic Society 93(10) (2010) 3486-3492.

[24] P. Duxson, G.C. Lukey, J.S.J. van Deventer, Physical evolution of Na-geopolymer derived from metakaolin up to 1000 °C, Journal of Materials Science 42(9) (2007) 3044-3054.

[25] S.A. Bernal, R.M. de Gutierrez, A.L. Pedraza, J.L. Provis, E.D. Rodriguez, S. Delvasto, Effect of binder content on the performance of alkali-activated slag concretes, Cement and Concrete Research 41(1) (2011) 1-8.

[26] T.W. Cheng, J.P. Chiu, Fire-resistant geopolymer produced by granulated blast furnace slag, Minerals Engineering 16(3) (2003) 205-210.

[27] İ. Türkmen, M.B. Karakoç, F. Kantarcı, M.M. Maraş, R. Demirboğa, Fire resistance of geopolymer concrete produced from Elazığ ferrochrome slag, Fire and Materials (2016) n/a-n/a.

[28] N.W. Chen-Tan, A. van Riessen, C.V. Ly, D.C. Southam, Determining the Reactivity of a Fly Ash for Production of Geopolymer, Journal of the American Ceramic Society 92(4) (2009) 881-887.

[29] W.D.A. Rickard, R. Williams, J. Temuujin, A. van Riessen, Assessing the suitability of three Australian fly ashes as an aluminosilicate source for geopolymers in high temperature applications, Materials Science and Engineering: A 528(9) (2011) 3390-3397.

[30] J.P. Boyd, Chebyshev & Fourier spectral methods, Berlin ; New York : Springer-Verlag, c1989.1989.

[31] I. Ismail, S.A. Bernal, J.L. Provis, S. Hamdan, J.S.J. van Deventer, Drying-induced changes in the structure of alkali-activated pastes, Journal of Materials Science 48(9) (2013) 3566-3577.

[32] Y. Ma, J. Hu, G. Ye, The pore structure and permeability of alkali activated fly ash, Fuel 104 (2013) 771-780.

[33] O.A. Abdulkareem, A.M. Mustafa Al Bakri, H. Kamarudin, I. Khairul Nizar, A.e.A. Saif, Effects of elevated temperatures on the thermal behavior and mechanical performance of fly ash geopolymer paste, mortar and lightweight concrete, Construction and Building Materials 50 (2014) 377-387.

[34] R.R. Lloyd, J.L. Provis, J.S.J. van Deventer, Microscopy and microanalysis of inorganic polymer cements. 2: the gel binder, Journal of Materials Science 44(2) (2009) 620-631.

[35] W.D.A. Rickard, A.v. Riessen, P. Walls, Thermal Character of Geopolymers Synthesized from Class F Fly Ash Containing High Concentrations of Iron and α-Quartz, International Journal of Applied Ceramic Technology 7(1) (2010) 81-88.

[36] W.D.A. Rickard, J. Temuujin, A. van Riessen, Thermal analysis of geopolymer pastes synthesised from five fly ashes of variable composition, Journal of Non-Crystalline Solids 358(15) (2012) 1830-1839.

[37] J.L. Provis, C.Z. Yong, P. Duxson, J.S.J. van Deventer, Correlating mechanical and thermal properties of sodium silicate-fly ash geopolymers, Colloids and Surfaces A: Physicochemical and Engineering Aspects 336(1–3) (2009) 57-63.

[38] S.A. Bernal, E.D. Rodríguez, R. Mejía de Gutiérrez, M. Gordillo, J.L. Provis, Mechanical and thermal characterisation of geopolymers based on silicate-activated metakaolin/slag blends, Journal of Materials Science 46(16) (2011) 5477.

[39] P. Duxson, G.C. Lukey, F. Separovic, J.S.J. van Deventer, Effect of Alkali Cations on Aluminum Incorporation in Geopolymeric Gels, Industrial & Engineering Chemistry Research 44(4) (2005) 832-839.

[40] C.E. White, J.L. Provis, L.E. Gordon, D.P. Riley, T. Proffen, J.S.J. van Deventer, Effect of Temperature on the Local Structure of Kaolinite Intercalated with Potassium Acetate, Chemistry of Materials 23(2) (2011) 188-199.

[41] P. Duxson, G.C. Lukey, J.S.J. van Deventer, The thermal evolution of metakaolin geopolymers: Part 2 – Phase stability and structural development, Journal of Non-Crystalline Solids 353(22–23) (2007) 2186-2200.

[42] P. Duxson, J.L. Provis, G.C. Lukey, S.W. Mallicoat, W.M. Kriven, J.S.J. van Deventer, Understanding the relationship between geopolymer composition, microstructure and mechanical properties, Colloids and Surfaces A: Physicochemical and Engineering Aspects 269(1–3) (2005) 47-58.

[43] B. Walkley, R. San Nicolas, M.-A. Sani, J.D. Gehman, J.S.J. van Deventer, J.L. Provis, Phase evolution of Na2O-Al2O3-SiO2-H2O gels in synthetic aluminosilicate binders, Dalton Transactions 45(13) (2016) 5521-5535.

[44] B. Walkley, R. San Nicolas, M.-A. Sani, G.J. Rees, J.V. Hanna, J.S.J. van Deventer, J.L. Provis, Phase evolution of C-(N)-A-S-H/N-A-S-H gel blends investigated via alkali-activation of synthetic calcium aluminosilicate precursors, Cement and Concrete Research 89 (2016) 120-135.

[45] O. Arioz, Effects of elevated temperatures on properties of concrete, Fire Safety Journal 42(8) (2007) 516-522.

[46] A. Kashani, R. San Nicolas, G. Qiao, J.S.J. van Deventer, J. Provis, Modelling the yield stress of ternary cement–slag–fly ash pastes based on particle size distribution, Powder technology 266 (2014) 203-209.

[47] J.B. Odelson, E.A. Kerr, W. Vichit-Vadakan, Young's modulus of cement paste at elevated temperatures, Cement and Concrete Research 37(2) (2007) 258-263.

[48] L. Alarcon-Ruiz, G. Platret, E. Massieu, A. Ehrlacher, The use of thermal analysis in assessing the effect of temperature on a cement paste, Cement and Concrete Research 35(3) (2005) 609-613.

[49] C. Alonso, L. Fernandez, Dehydration and rehydration processes of cement paste exposed to high temperature environments, Journal of Materials Science 39(9) (2004) 3015-3024.